Virtual experimentation for EMC parameters extraction : case of the parasitic capacitance in wound structures

Ioav Ramos, Jean-Marc Diénot, Paul-Etienne Vidal, Bertrand Nogarède, Christophe Viguier, Emmanuel Batista

VIRTUAL EXPERIMENTATION FOR EMC PARAMETERS EXTRACTION: CASE OF THE PARASITIC CAPACITANCE IN WOUND STRUCTURES

J. I. Ramos[1,2], J-M. Diénot[2], P-E. Vidal[2], B. Nogarède[1], C. Viguier[1], E. Batista[3]

1. NOVATEM SAS, Advanced Mechatronics, 3 rue Merlin de Thionville, 11111 Coursan, France
e-mail: ji.ramos@novatem-sas.com

2. LGP, ENIT-INP, Toulouse University, 47 av. d'Azeirex, 65000 Tarbes, France

3. ALSTOM Transport, 50 Rue du Docteur Guinier, 65600 Séméac, France

Abstract - A new method for analyzing the impact of materials and architectures of Power Mechatronic assemblies on the parasitic electromagnetic couplings is presented. In this paper, the stray capacitance of a single-layer iron-core solenoid is analyzed using a PEEC-based 3D method. The results are compared to an analytical calculation of turn-to-turn and turn-to-core capacitance to validate the proposed method. The solenoid is subject to an EM field calculation in order to extract the coupling coefficients between different turns and the core of the inductor. The coupling coefficient matrix is extracted and imported into a Netlist circuit formalism for further analysis and comparison with the analytical calculations. These first derived results will be helpful in the modeling works for solving EMC issues such as transient over-voltage in wound structures of power Mechatronic systems. This is a first step of The Virtual Experimentation Method for future analyzing and designing of compatible Mechatronic subsystems, by integrating materials and architecture parameters into the design process.

Keywords Power Components, Mechatronic Systems, Parasitic Couplings, Partial Element, Stray Capacitance, Virtual Experimentation, EMC.

1. INTRODUCTION

1.1. EMC ANALYSIS OF COMPLEX ELECTRICAL SYSTEMS

The current development of Mechatronic Embedded systems leads to optimize the efficiency of electromechanical actuators associated to their power electronics and cablings. Consequently, the power-to-weight ratio constraints, the increasing nominal and switching frequencies and the integration challenges on geometrical dimensions contribute to new severe electromagnetic interferences (EMI) within the mechatronic assemblies. These cases of new potential perturbations modify the conventional state-of-the-art methods of driving and monitoring of coupling modes of the system, for Electromagnetic Compatibility (EMC) issues, in order to avoid disturbances scenarios.

Common mode and differential mode impedance analysis of the assembly is a usual and efficient way to have good prediction of the EMC behavior of the machine and the inverter [1]. For instance, several high-frequency models of induction and synchronous motors' per-phase impedance at a system level have been developed to satisfy good EMC-design criteria's of integrated Mechatronic systems, up to 100 MHz [2][3].

Based on identification process, measurements of common mode and differential mode impedance of synchronous and induction machines allow the parameterization for time and frequency domain simulations [1]. Models are fitted to measurements by identifying significant points in the impedance plot and relating them, when possible, to actual winding parameters [1],[4],[5]. Unfortunately, the optimal model tuning is obtained when some parameters not directly related with winding parameters are introduced. Moreover, these same parameters, for different machines, do not correlate to general trends of increasing rated power nor size [1].

Thus, it seems very difficult to predict EMC behavior between the inverter and the machine, from the design phase, when both machine and inverter are co-designed for Mechatronic purposes, and with new higher frequency uses. Finally, mainly conducted EMI is taken into account, but it

has been shown now that near-field radiation in modern power electronics becomes critical, with high frequencies and high switching rates [6].

1.2. EMC PREDICTION AND EMC DESIGN

Accessing to constitutive parameters of electromechanical actuators and inverter is essential for calculation and prevision of emission and coupling's behavior at advanced design stages. This concerns materials' properties, specific geometries, temperature, electromagnetic environment and physical layout of machine components among others. Simulation at a system level is very pertinent for understanding fine physical behaviors, but is not efficient nor versatile, especially for early steps of design, where parameters are not still fixed. Circuit simulations allow efficient time and frequency analysis of complex electromagnetic systems with short simulation times.

In this paper, we propose to link these two domains with a main effort on pertinent parameter extraction and circuit simulation for EMC design. These comprehensive approaches, named Virtual Experimentation for EMC (XVICE), allow optimal electromagnetic behavior prediction for complex electrical structures [7]. It allows the designer to analyze the impact of structure or material modifications in the design process, to take into account the potential effects of couplings between components, and to simulate them in a system circuit analysis. The method is mainly adapted from the use of the Partial Element Equivalent Circuit (PEEC) concept [8] . The PEEC method is based on 3D electromagnetic calculations, and gives parameter's value of equivalent RLC cells, that have been meshed in the geometry and with the materials of the structure. We propose to start the study on iron core solenoid used in new Mechatronic application, to derive more appropriate modeling of parasitic elements as capacitance in Wound structures. The first comparison and validation with experimental and analytical approaches will be discussed, based on a formal case study.

2. THE PARTIAL ELEMENT EQUIVALENT CIRCUIT (PEEC) METHOD AND APPLICATION

2.1. THE PARTIAL ELEMENTS METHOD

The PEEC theory was developed by A. Ruehli in 1972, and the theory has had multiple contributions throughout last two decades [8],[9],[10]. PEEC method is based on an integral electromagnetic formulation describing the geometry and interpreted in terms of L, C, and R circuit elements. It provides a correlation of the field calculation and the circuit interpretation [10]. Summation of all sources of electric field within a conductor leads to the expression of the external field applied:

$$\vec{E}_0 = \frac{\vec{J}(\vec{r},t)}{\sigma} + \frac{\vec{\partial A}(\vec{r},t)}{\partial t} + \nabla\Phi(\vec{r},t) \tag{1}$$

Where $\vec{r}$ is the vector from the origin and $\vec{E}_0$ an external field. Introducing the expressions of vector potential and scalar potential [11] for a system of K conductors and regions of uniform ε_r, μ_r; c being the speed of light:

$$\begin{aligned}\vec{E}_0 &= \frac{\vec{J}(\vec{r},t)}{\sigma} \\ &+ \sum_{k=1}^{K} \frac{\vec{\partial}}{\partial t}\left[\frac{\mu}{4\pi}\int_{vk} G(\vec{r},\vec{r}')\vec{J}(\vec{r}',t')dv'\right] \\ &+ \sum_{k=1}^{K} \nabla\left[\frac{1}{4\pi\varepsilon}\int_{vk} G(\vec{r},\vec{r}')q(\vec{r}',t')dv'\right]\end{aligned} \tag{2}$$

Where $G(\vec{r},\vec{r}') \equiv \frac{1}{|\vec{r}-\vec{r}'|}$ (3)

t' is considered to be the retardation time between the source point $\vec{r}'$ and the observation point $\vec{r}$. The unknown quantities then are the current density J in conductors and density of charges q on the surfaces. In order to solve the system of equations derived from (2), current densities are discretized into N volume cells, giving the overall current flow for each one of K conductors, then by defining local cell current densities as a pulse function in the three dimensional directions $\gamma = x, y, z$ [8][11]. As for the density of charges, they are defined on the conductor surfaces and expressed as pulse functions as well for M surface cells. In the case of perfect conductors for capacitance calculation, absence of external electric field and aforementioned unknown quantities being locally constant (more general cases are detailed in [9],[10]), integrating the volume of the l^{th} cell of the K conductors leads to:

$$\begin{aligned}0 &= \frac{1}{\sigma}\int_{v_l} \vec{J}_{\gamma}(\vec{r},t)dv_l \\ &+ \sum_{k=1}^{K}\sum_{n=1}^{N_{\gamma k}} \frac{\mu}{4\pi}\left[\int_{v_l}\int_{vnk} G(\vec{r},\vec{r}')dv'dv_l\right]\frac{\partial \vec{J}_{\gamma nk}(t_n)}{\partial t} \\ &+ \sum_{k=1}^{K} \frac{1}{4\pi\varepsilon}\int_{v_l}\frac{\partial}{\partial\gamma}\left[\int_{vk} G(\vec{r},\vec{r}')q(\vec{r}',t')ds'\right]dv_l\end{aligned} \tag{4}$$

t_n is an approximation of t'. Each term of (4) can be identified as $0 = v_R + v_L + v_C$. The first term in the right-hand side is then interpreted as the resistive voltage drop along the γ direction of cell l:

$$v_R = \boldsymbol{R}_{\gamma l} \boldsymbol{I}_{\gamma l} \tag{5}$$

The term in brackets of second term on the right-hand side of (4) is recognized as the partial inductance multiplied by the cross section of the cell perpendicular to the current flow a_l and to the cross section of the n^{th} cell of the k^{th} conductor in the γ direction, $a_{\gamma mk}$. The inductive voltage drop is finally recognized as:

$$v_L = \sum_{k=1}^{K} \sum_{n=1}^{N_{\gamma k}} \boldsymbol{Lp}_{l,\gamma mk} \frac{d\boldsymbol{I}_{\gamma mk}(t_n k)}{dt} \tag{6}$$

Lp are the partial (self and mutual) inductances for every cell of the conductor. Similar identifications can be conducted for partial capacitance using a finite difference approximation (FD) [11]. The voltage drop caused by capacitive impedance can then be written as follows:

$$v_C = \sum_{k=1}^{K} \sum_{m=1}^{M_{\gamma k}} \boldsymbol{Q}_{mk}(t_{mk}) \left[\boldsymbol{pp}_{mk}^{+} - \boldsymbol{pp}_{mk}^{-} \right] \tag{7}$$

Here, Q_{mk} is the total charge on the *mkth* cell and pp_{mk} partial coefficients of potential for the positive and negative leads of the cells. Multicapacitances can then be extracted as $cp = pp^{-1}$ [9].

2.2. Partial Elements Extraction

The calculation of partial elements is done for each one of the discretized volume/surface cells and arranged into a partial element matrix containing self-partial elements and couplings between cells as showed in Fig. 1.

The software used for partial element extraction is a PEEC-based electromagnetic software for frequency-fixed simulations: Q3D Extractor [12]. It is a complete multi-material simulator taking into account resistive conductors and lossy dielectrics. Ports are defined for physically separated conductors only. Every conductor is assigned with a net name and an excitation (source and sink on isolated faces of the conductor) for simulation. A conductor not assigned with an excitation is considered to be grounded. Every conductor can be virtually segmented in several volume and surface cells for time delay considerations.

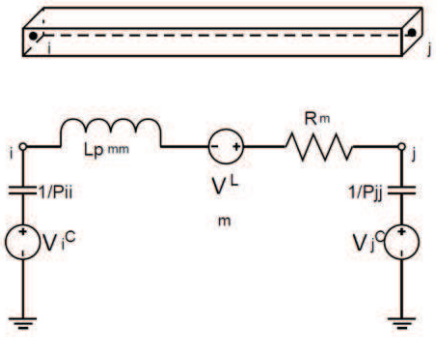

Fig. 1. PEEC model for volume cell m of the kth conductor connecting node i and j [9].

The three matrixes of the values corresponding to Resistive (R), Inductive (L) and Capacitive (C) behavior of the structure, can be are exported in a SPICE Netlist formalism, containing the circuit arrangement with the partial elements and couplings. The Netlist is then imported as a subcircuit whose ports are functional conductors or nets defined in the 3D model and connected to a larger circuit for larger circuit analysis.

$$C_k = \begin{bmatrix} c_1 & \Lambda & c_{1j} & c_{1M} \\ \mathrm{M} & \mathrm{O} & & \mathrm{M} \\ c_{i1} & & c_i & \mathrm{M} \\ c_{M1} & \Lambda & \Lambda & c_M \end{bmatrix} \qquad C_T = \begin{bmatrix} C_1 & \Lambda & C_{1j} & C_{1K} \\ \mathrm{M} & \mathrm{O} & & \mathrm{M} \\ C_{i1} & & C_i & \mathrm{M} \\ C_{K1} & \Lambda & \Lambda & C_K \end{bmatrix}$$

(a) (b)

Fig. 2. Capacitance matrix of partial self and mutual capacitance of every surface cell of a conductor k (a). Capacitance matrix of the partial self and mutual capacitances of K conductors (ports) (b).

The total capacitance matrix is exported as a SPICE format Netlist.

3. Description of the Case Study : A Solenoid

The solenoid simulated is a single layer iron-cored solenoid with 7 jointed turns. Dimensions of the solenoid are given in Table I and Fig. 3. Material properties are resumed in table II.

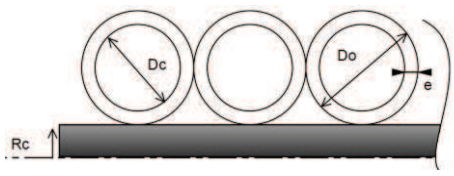

Fig. 3. Solenoid layout

I. Solenoid Dimensions

Rc	Iron core radius	10 mm
Lc	Iron core length	18 mm
Dc	Copper wire diameter	1.5 mm
Do	Outer diameter of wire	1.6 mm
e	Coating thickness	0.05 mm

II. Material Properties

Conductivity of copper	σ_c=58 000 000 S/m
Relative permeability of copper	μ_c=0.99991
Relative permittivity of coating material	ε_r=3.5
Relative permeability of iron core	μ_i=4000
Conductivity of iron core	σ_i=10 300 000 S/m

The physical dimensions being short to electrical dimensions, the propagation effects are not taken into account and only one volume cell per conductor is modeled. For capacitance matrix calculation, Q3D considers the copper and iron to be perfect conductors. The functional conductors are thus defined as nets. Every turn is electrically isolated from one another and defined as a net. In this study, an emphasis is done on the capacitance calculation. Effects of frequency are thus neglected.

3.1. Analytical Calculation of Capacitance Matrix

3.1.1 General modeling and considerations

To compare the results of the virtual experimentation on the solenoid, analytical calculations of turn-to-turn and turn-to-core capacitance have been carried out. Three couplings are identified:

- Turn-to-turn capacitance of the same layer
- Turn-to-turn capacitance for turns of different layers
- Turn-to-core capacitance.

Fig. 4 shows the cross sectional view of a multilayer solenoid. Because of symmetries, electric field lines must be equally shared between adjacent conductors [13]. For the last layer, we assume the lines to be shared equally between the two adjacent turns as a first approximation.

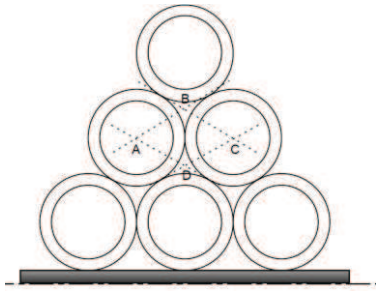

Fig. 4. Cross section of a multilayer solenoid.

The calculation of turn-to-turn capacitance can be reduced to the analysis of the ABCD cell representing the assumed electric field lines mean paths between two turns [14].

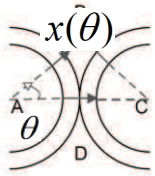

Fig. 5 Assumed path *x* for field lines between adjacent conductors for $-\pi/6 \leq \theta \leq \pi/6$.

These results are validated for single and multiple layers windings. In [14], results of self-resonant frequency measurements were carried out. The error in determining self-capacitance was of -17.2% for the solenoid modeled.

3.1.2 Turn-to-turn capacitance

Electric field lines are orthogonal to the conductor surfaces since surfaces are considered to be perfect equipotentials. The paths are then depicted for the field lines: lines from one turn to another go through a coating thickness, then trough air and through coating thickness again. Since the thickness *e* is small to wire diameter *Dc*, lines in the coatings are considered to be orthogonal to the conductor surface as shown in Fig 5. Because of the proximity effect, electric field lines are concentrated around the shortest distance between two different equipotentials. Thus, E lines are considered to be parallel and close to small values of θ as show in Fig. 5. It is then assumed that for adjacent turns, the flux lines are exclusively directed towards the next immediate conductor.

The elementary capacitance *dC* between the equivalent elementary surfaces *dS* of two adjacent conductors can then described as in (8) [17].

$$dC = \varepsilon \frac{dS}{x} \tag{8}$$

The capacitance along the first path (coating of the first turn) can then be calculated:

$$dCc = \varepsilon_r \varepsilon_0 \frac{r}{dr} d\theta dl \tag{9}$$

$$dCc = \varepsilon_r \varepsilon_0 d\theta \int_0^{lt} dl \int_{r_c}^{r_0} \frac{r}{dr} \tag{10}$$

So that

$$dCc = \varepsilon \frac{lt}{\ln\left(\frac{r_0}{r_c}\right)} d\theta \tag{11}$$

In numerical calculations, the length of a turn *lt* is here approximated to its perimeter. For the air gap, the capacitance can be calculated considering that in this region, x*(θ)=Do(1-cosθ)*.

$$dCg = \varepsilon_0 \frac{lt}{2(1-\cos\theta)} d\theta \tag{12}$$

Finally, for the third segment concerning E lines entering the coating of the second conductor, the capacitance is the same as in (11), as for the first coating. Thus, the total turn-to-turn capacitance can be written as *Ctt=2*Cc+Cg.*

3.1.3 Turn-to-core capacitance

For the inner layer, the turn-to core capacitance can easily be calculated with the same expressions. Considering the iron core surface as a perfect equipotential, electric field lines are orthogonal to the surface of the core. In that case, turn-to-core electric field lines go through half of the path compared to the turn-to-turn lines [13],[15]. The resulting capacitance is then $C\ t=2C\ t$ integrating for all values of θ ($-\pi/6 \le \theta \le \pi/6$). The matrix of capacitance C is then easily determined as described in Fig. 2.

3.2. RESULTS

Turns are numbered from 1 to 7 and core is identified with number 0. The concerned capacitance arrangements are shown in Fig. 6.

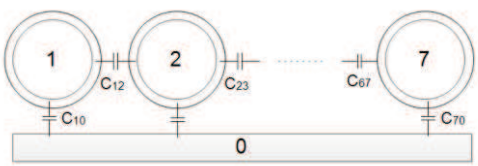

Fig. 6 Identification of calculated on the structure.

The analytical computation leads to a turn-to-turn capacitance value of 7.65 pF. The turn-to-core is then 15.3 pF. Using the Q3D capacitance extraction the results are expressed in Tables III and IV.

III. Extracted turn-to-turn capacitance compared to analytical calculations

Turn-to-turn capacitance Ctt	Absolute value pF
C_{12}	7.19
C_{23}	7.47
C_{34}	7.21
C_{45}	7.29
C_{56}	7.41
C_{67}	7.22
Mean extracted Ctt	**7.30**

Comparing the analytical results and the average computed value of turn-to-turn capacitance the relative error is 4.57%.

IV. Extracted turn-to-core capacitances compared to analytical calculations

Turn-to-core capacitance Ctc	Absolute value pF
C_{10}	7.29
C_{20}	7.50
C_{30}	7.19
C_{40}	7.39
C_{50}	7.02
C_{60}	7.18
C_{70}	8.01
Mean Ctc	**7.37**

The relative error compared to the analytical calculation is 52%. The ratio between turn-to-turn and turn-to-core capacitance values is 1 which isn't in accordance with the prediction of a ratio of 2 predicted by the analytical calculations.

Results extracted by PEEC method of to turn-to-turn capacitance were consistently stable and in accordance with analytical predictions. However, turn-to-core capacitance extractions were unstable for different simulations. Results were highly unstable and weren't in accordance with analytical predictions. Conclusions about these discrepancies are being evaluated. Q3D® and its meshing algorithm are not optimized for toroidal and helical structures with thin coats of materials. They were

originally built to test PCB structures and IC packaging.

Turn-to-turn capacitance simulation for immediate non-adjacent turns was also analyzed and compared to turn-to-turn capacitance as presented in Table V. This result is in accordance with the analytical approximation in which electric field lines are mostly shared between adjacent turns or core.

V. Immediate non-adjacent turns capacitance comparison

Turn-to-turn capacitance for immediate non-adjacent turns Ct(t+2)	Absolute value pF
C_{13}	0.037
C_{24}	0.051
C_{35}	0.01
C_{46}	0.022
C_{57}	0.017
Mean	**0.028**
Mean Ctt	**7.65**
Ratio	**280**

4. CONCLUSIONS

In the first paragraph, a description of the needs and existing EMC-efficient design tools was pointed out. In the second part, the PEEC method is highlighted. Finally XVICE method was described in part 3 and some comparison results extracted from PEEC method and analytical calculation are discussed. Results are encouraging for turn-to-turn capacitance. Turn-to-core capacitance extraction results were not conclusive but further work is being carried out to determine if the simulation conditions can be improved and compared with other methods such as Finite Element calculations.

ACKNOWLEDGEMENTS

Scientific resources for this work have been supported by the EMI/EMC Plat-form LABCEEM, University P. Sabatier, FR-65000 Tarbes. http://labceem.iut-tarbes.fr, jm.dienot@iut-tarbes.fr

REFERENCES

[1] S. Weber, E. Hoene, S. Guttowski, W. John, H. Reichl, Modeling Induction Machines for EMC-Analysis. Power Electronics Specialists Conference, 2004. PESC '04, IEEE 35th Annual

[2] M. Schinkel, S. Weber, S. Guttowski, W. John, Efficient HF Modeling and Model Parameterization of Induction Machines for Time and Frequency Domain Simulations. Applied Power Electronics Conference and Exposition, 2006. APEC '06, 21st annual IEEE.

[3] J. Luszcz, K. Iwan, Conducted EMI Propagation in Inverter-fed AC Motor. Electrical Power Quality and Utilisation Magazine Vol. II, No. 1, 2006.

[4] E. Zhong, T. Lipo, Improvements in EMC Performance of Inverter-fed Motor Drives. IEEE Transactions in Industry Applications, 1995.

[5] G. Grandi, D. Casadei, U. Reggiani, Analysis of Common-Mode and Differential-Mode HF Current Components in PWM Inverter-fed AC Motors, Power Electronics Specialists Conference, 1998. 29th annual IEEE.

[6] E. Batista, J.M. Dienot, "EMC characterizations for Switching Noise Investigation on Power Transistors", IEEE International Symposium on Electromagnetic Compatibility, Detroit, USA, August 18-23, 2008.

[7] J.M. Dienot, E. Batista, J.L. Massol, "Virtual Experiment for Interferences and Electromagnetic Compliances : simulations of new real-case electromagnetic behavior in hybrid embedded electronics with temperature impact", IEEE International Workshop on EM methods, ST Malo, France, December 2-3, 2010

[8] A. E. Ruehli, Equivalent Circuit Models for Three-Dimensional Multiconductor Systems, IEEE Transactions on Microwave Theory and Techniques, 22(3):216–221, March 1974.

[9] A. E. Ruehli, Circuit Models for Three-Dimensional Geometries Including Dielectrics, IEEE transactions on Microwave Theory and Techniques, 40(7):1507–1516, July 1992.

[10] G. L. Li, Z.-H. Feng, "Consider the Losses of Dielectric in PEEC", Int. Conference on Microwave and Millimeter Wave Technology Proceedings, pages 793–796, Beijing, China, 2002.

[11] A. F. Peterson, S. L. Ray, and R. Mittra, Computational Methods for Electromagnetism. IEEE Press, New York, USA, 1998.

[12] Q3D Technical Notes, MAXWELL 3D Extractor Technical Notes, ANSOFT, 2001.

[13] A. Massarini M.K. Kazimierczuk, G. Grandi, Lumped Parameter Models for Single- and Multiple-Layer Inductors, Power Electronics Specialists Conference, 1996. 27th annual IEEE.

[14] A. Massarini, M. K. Kazimierczuk, Self-Capacitance of Inductors, IEEE Transactions on Power Electronics, vol. 12 issue 14, 2002

[15] l. Dalessandro, F. da Silveira, J. W. Kolar, Self-Capacitance of High-Voltage Transformers. IEEE Transactions on Power Electronics, vol. 22 issue 5, 2007